

Physics-Informed Neural Networks: Minimizing Residual Loss with Wide Networks and Effective Activations

Nima Hosseini Dashtbayaz¹, Ghazal Farhani^{2,*}, Boyu Wang^{1,3,*} and Charles X. Ling¹

¹Department of Computer Science, University of Western Ontario

²National Research Council of Canada

³Vector Institute

nhosse5@uwo.ca, ghazal.farhani@nrc-cnrc.gc.ca, bwang@csd.uwo.ca, charles.ling@uwo.ca

Abstract

The residual loss in Physics-Informed Neural Networks (PINNs) alters the simple recursive relation of layers in a feed-forward neural network by applying a differential operator, resulting in a loss landscape that is inherently different from those of common supervised problems. Therefore, relying on the existing theory leads to unjustified design choices and suboptimal performance. In this work, we analyze the residual loss by studying its characteristics at critical points to find the conditions that result in effective training of PINNs. Specifically, we first show that under certain conditions, the residual loss of PINNs can be globally minimized by a wide neural network. Furthermore, our analysis also reveals that an activation function with well-behaved high-order derivatives plays a crucial role in minimizing the residual loss. In particular, to solve a k -th order PDE, the k -th derivative of the activation function should be bijective. The established theory paves the way for designing and choosing effective activation functions for PINNs and explains why periodic activations have shown promising performance in certain cases. Finally, we verify our findings by conducting a set of experiments on several PDEs. Our code is publicly available at https://github.com/nimahsn/pinns_tf2.

1 Introduction

The success of deep learning in a wide variety of tasks has motivated its application in scientific domains as well [Sirignano and Spiliopoulos, 2018; Reiser *et al.*, 2022; Li *et al.*, 2020]. PINNs [Raissi *et al.*, 2017] in particular are designed to solve differential equations as an alternative to traditional solvers, benefiting from discretization-free construction and the vast availability of machine learning tools and techniques. As a result, PINNs have been deployed in various physics and engineering problems, such as solving inverse scattering problems in photonics [Chen *et al.*, 2020a], flow problems in

fluid dynamics [Cai *et al.*, 2021], and computational neuromusculoskeletal models raised in biomedical and rehabilitation sciences [Zhang *et al.*, 2022].

Consider a general-form PDE with a Dirichlet boundary condition such as

$$\begin{aligned} \mathcal{D}[u](x) &= f(x) & x \in \Omega \\ u(x) &= g(x) & x \in \partial\Omega, \end{aligned} \quad (1)$$

where u is the solution of the PDE on a bounded domain $\Omega \subset \mathbb{R}^d$ of d independent variables with boundaries $\partial\Omega$, f and g are known functions, and \mathcal{D} is a differential operator. Here, the operator \mathcal{D} expresses the physical rules governing u through a differential expression. PINNs are then trained to respect the underlying physical dynamics given in \mathcal{D} by minimizing the residual loss

$$L_r = \sum_{x \in \mathbf{x}} l(\mathcal{D}[\hat{u}](x) - f(x)), \quad (2)$$

where \hat{u} is a neural network approximation of u , l is an error function such as squared error, and \mathbf{x} is a set of training collocation points in Ω . To guarantee a unique solution, boundary (and initial) conditions are also imposed by adding other supervised loss terms, referred to as boundary loss, trained with boundary data sampled from $\partial\Omega$. The resulting loss function can then be treated as a multi-objective optimization task [Raissi *et al.*, 2017].

While proven effective, training PINNs is often a challenging task. These challenges usually originate from either the discrepancy between the residual loss and the boundary loss [Wang *et al.*, 2020b; Farhani *et al.*, 2022; Wang *et al.*, 2020a] or the nature of the residual loss [Krishnapriyan *et al.*, 2021; Wang *et al.*, 2022]. Notably, as Eq. 2 involves differentiation over a neural network with respect to (w.r.t.) its inputs, the outputs of the network undergo a significant structural transformation. To better understand the aforementioned process and its implications, let us consider a simple differential operator $\frac{\partial u}{\partial x}$ of a single independent variable and an L -layer feed-forward network with an activation function σ . One can find that the application of this differential operator on the neural network, $\mathcal{D}[\hat{u}]$, is given by

$$\mathcal{D}[\hat{u}] = W_L^\top \times (\sigma'(G_{L-1}) \circ W_{L-1})^\top \times \cdots \times (\sigma'(G_1) \circ W_1)^\top, \quad (3)$$

where W_i and G_i are weights and linear outputs of layer i , and \circ and \times denote element-wise (Hadamard) and matrix

*Corresponding Author

products. In contrast, the original neural network \hat{u} can be defined recursively as

$$\hat{u}(x) = G_L(x), \quad G_i(x) = \sigma(G_{i-1}(x)) \times W_i + b_i.$$

Eq. 3 shows how the differentiation transforms the outputs of a neural network. Firstly, note that the simple recursive relation between the layers of a feed-forward network is disrupted by applying \mathcal{D} , and additional element-wise products with weights emerge as well. More significantly, we observe that the derivative σ' of the activation function appears in the outputs. This presence of σ' in PINNs highlights the importance of an activation function with well-behaved derivatives in the model’s expressive power in learning \mathcal{D} and likewise in the optimization process as it involves higher-order derivatives of σ .

Altogether, the distinct characteristics of $\mathcal{D}[\hat{u}]$ and the resulting residual loss, contribute to a problem that is quite different from common supervised training tasks. Consequently, the existing theory around loss functions and their characteristics cannot readily be applied to PINNs, and the lack of understanding about PINNs and their optimization dynamics leads to uninformed design choices and suboptimal performance even for seemingly easy PDEs.

In this work, we focus on the residual loss and its landscape. Specifically, we are interested in finding what neural networks and design choices enable PINNs to globally minimize the residual loss. To this end, we study the residual loss at a critical point of the network parameter space and search for distinctive characteristics of a global minimum compared to other critical points. Once these characteristics are identified, our investigation shifts towards determining sufficient conditions within the network design, in particular, width and activation function, that guarantee the existence of global minima in the parameter space. Our findings underscore the importance of the width and activation functions with well-behaved high-order derivatives in acquiring a high expressive power in learning the differential operator. Finally, we verify our findings by conducting extensive experiments on several PDEs.

We summarize our contributions as follows. (1) We theoretically show that the residual loss of PINNs can be globally minimized, given a two-layer neural network with a width equal to or greater than the number of collocation points. (2) Through our analysis, we establish that the residual loss for a k -th order differential operator is optimally minimized when using an activation function with a bijective k -th order derivative. We leverage this theoretical foundation as a guideline for selecting activation functions, justifying the choice of sinusoidal activations, and subsequently validating their effectiveness through empirical demonstrations and experiments.

2 Related Works

2.1 Wide Neural Networks

Wide neural networks have historically been of significant interest in machine learning. With classical results such as Universal Approximation and Gaussian processes, and more recently, NTK theory [Jacot *et al.*, 2018], wide networks have been studied to understand neural networks in certain regimes

[Chen *et al.*, 2020b; Lee *et al.*, 2019]. The optimal width of a neural network is also studied for convergence guarantees [Oymak and Soltanolkotabi, 2020; Du *et al.*, 2019; Allen-Zhu *et al.*, 2019; Nguyen and Mondelli, 2020] and loss geometry [Safran and Shamir, 2016; Nguyen and Hein, 2017] with certain classes of neural networks and optimizers. The convergence guarantees are often provided for a width polynomial in the number of training samples and the number of layers [Allen-Zhu *et al.*, 2019]. Safran and Shamir [2016] studied the basins of the loss function for wide two-layer ReLU networks, showing that wider networks are initialized at a good basin with higher probability. [Nguyen and Hein, 2017] also showed that most of the critical points in a wide neural network are also global minima. The developed theory in most of the aforementioned works cannot be directly applied to PINNs, as they either rely on specific neural network formulations [Nguyen and Hein, 2017; Nguyen and Mondelli, 2020], which are disrupted by differentiation, or certain hyper-parameters that are not effective for PINNs, such as ReLU activation function [Du and Hu, 2019; Safran and Shamir, 2016; Allen-Zhu *et al.*, 2019].

2.2 Periodic Activation Functions

Sitzmann *et al.* [2020] proposed using sinusoidal activation functions in neural networks with low-dimensional inputs for learning differentiable signals. Notably, they also showed the capability of Sine networks in solving Wave and Helmholtz PDEs with PINNs. Since then, few works have explored the behaviour of neural networks with periodic activation functions at initialization [Belbute-Peres and Kolter, 2022] and their expressive power as function approximators [Meronen *et al.*, 2021]. Meronen *et al.* [Meronen *et al.*, 2021] studied the inductive bias introduced by periodic activation functions on the neural network functional space, and showed that such networks are less sensitive to input shifts.

2.3 Physics-Informed Neural Networks

Besides the applications of PINNs in solving various PDEs, there has been a surge in analyzing the behaviour and pitfalls of PINNs in recent years, especially from the optimization perspective [Wang *et al.*, 2020a; Liu *et al.*, 2020; Farhani *et al.*, 2022]. Using *Neural Tangent Kernel* (NTK) theory from infinitely wide neural networks, [Wang *et al.*, 2020b] showed that high-frequency terms in a PDE result in discrepancies in the convergence rate between the loss objectives when trained with Gradient Descent, leading the model to exhibit behaviours similar to spectral bias [Rahaman *et al.*, 2018]. Wang *et al.* [2020a] also showed similar results by studying the magnitude of the loss gradients at different layers. Later on, the momentum term was shown to address the discrepancy in optimization in the infinite-width regime [Farhani *et al.*, 2022].

Many recent works alleviate the optimization challenges in PINNs and improve their performance by assigning weights to each loss term [Wang *et al.*, 2020b; McClenny and Braganeto, 2020; Wight and Zhao, 2020], designing new architectures and embeddings [Wong *et al.*, 2022; Wang *et al.*, 2020a; Wang *et al.*, 2021; Dong and Ni, 2021], and using sophisticated training strategies such as curriculum learning [Kr-

ishnapriyan *et al.*, 2021; Wang *et al.*, 2022]. Among them, [Wang *et al.*, 2020b] and [Wong *et al.*, 2022], suggested mapping the inputs to random or trainable Fourier features and the use of sinusoidal activation functions to overcome the spectral bias and the convergence discrepancy.

3 Global Minima of the Residual Loss

In this section, we study the residual loss at its critical points to obtain sufficient conditions for the existence of global minima. We present the proofs for the lemmas and theorems in this section in the Appendix. First, we introduce the notation and the setup used throughout this section.

3.1 Notation and Setup

We use $\hat{u}_{\mathcal{W}} : \mathbb{R}^d \times \mathbb{R}^{|\mathcal{W}|} \rightarrow \mathbb{R}^{n_L}$ to denote an L -layer feed-forward neural network parameterized by $\mathcal{W} = \{W_i, b_i \mid 1 \leq i \leq L, W_i \in \mathbb{R}^{n_{i-1} \times n_i}, b_i \in \mathbb{R}^{n_i}\}$, where n_i is the number of neurons in layer i , $n_0 = d$, and $n_L = 1$. We drop \mathcal{W} from $\hat{u}_{\mathcal{W}}$ for simplicity if there is no ambiguity. The neural network \hat{u} for an input $x = (x_1, \dots, x_d)$ is formulated as

$$\begin{aligned} \hat{u}(x) &= G_L(x), \\ G_i(x) &= F_{i-1}(x) \times W_i + b_i \quad \forall i \in \{1, \dots, L\}, \\ F_i(x) &= \sigma(G_i(x)) \quad \forall i \in \{1, \dots, L-1\}, \end{aligned} \quad (4)$$

where σ is an activation function, and $F_0(x) = x$. We further define $F_i^{(k)}(x)$ as

$$F_i^{(k)}(x) = \sigma^{(k)}(G_i(x)),$$

where $\sigma^{(k)}$ is the k -th derivative of σ . In the case of $k = 1$, we simply use F_i' and σ' instead. For a batch \mathbf{x} of N samples, $F_i(\mathbf{x})$, $G_i(\mathbf{x})$, and $F_i^{(k)}(\mathbf{x})$ are $N \times n_i$ matrices. Also, the matrix power W^k represents an element-wise power.

In a PINN, the neural network \hat{u} is trained to approximate the solution u of a differential equation denoted as in Eq. 1. In this work, we assume that \mathcal{D} is a linear differential operator, i.e., the PDE is linear in the derivatives of u and u itself. We reformulate the residual loss in Eq. 2 to be a function of weights \mathcal{W} and choose $l(r) = r^2$.

$$\phi_r(\mathbf{x}; \mathcal{W}) = \sum_{x \in \mathbf{x}} l(\mathcal{D}[\hat{u}](x) - f(x)). \quad (5)$$

Throughout the rest of this section, we consider a two-layer neural network and a simple k -th order differential operator $\mathcal{D}[u] = \frac{\partial^k u}{\partial x^k}$ for a single independent variable x (i.e., $d = 1$). We generalize the results in this section to more independent variables in the Appendix.

3.2 Residual Loss of a Two-layer PINN

To study the residual loss and its critical points, we first need to derive the analytic formula for the residual loss and its gradients. The next two lemmas, provide us with these tools by finding the differentiation $\mathcal{D}[\hat{u}]$ and then deriving the gradients of the resulting residual loss.

Lemma 1. *For a two-layer neural network \hat{u} defined in Eq. 4, and a k -th order differential operator $\mathcal{D}[u] = \frac{\partial^k u}{\partial x^k}$ of a single independent variable x , $\mathcal{D}[\hat{u}]$ is*

$$\mathcal{D}[\hat{u}](x) = W_2^\top \times (F_1^{(k)}(x) \circ W_1^k)^\top.$$

With the analytic formula for $\mathcal{D}[\hat{u}]$ in hand, it is easy to plug it into Eq. 5 to get the residual loss. The next lemma derives the gradients $\nabla_{W_2} \phi_r(\mathbf{x}; \mathcal{W})$ of the residual loss w.r.t. the weights of the last layer.

Lemma 2. *For \hat{u} and $\mathcal{D}[\hat{u}]$ given in Lemma 1, gradients of the residual loss w.r.t. the weights of the second layer over the training collocation data \mathbf{x} of N samples are given by*

$$\nabla_{W_2} \phi_r(\mathbf{x}; \mathcal{W}) = W_1^k \circ [l'(\mathcal{D}[\hat{u}](\mathbf{x}) - f(\mathbf{x}))^\top \times F_1^{(k)}(\mathbf{x})].$$

Remark 1. Lemmas 1 and 2 generalize the appearance of derivatives in the outputs of the neural network as in Eq. 3, showing that a k -th order differential term similarly contains the k -th derivative of the activation function. Thus, activation functions with vanishing high-order derivatives, such as ReLU, significantly reduce the network representation power in approximating the residuals. Note that the gradients w.r.t. W_1 contain the $(k+1)$ -th derivative of the activation function, further highlighting the importance of well-behaved derivatives in optimization.

In the following section, the gradients given in Lemma 2 are studied at a critical point to find the characteristics of global minima of the residual loss. Note that global minimum in this context refers to the parameters that make the loss zero.

3.3 Critical Points of Wide PINNs

We are eventually interested in finding sufficient conditions for the existence of a global minimum of the residual loss, i.e., $\phi_r(\mathbf{x}; \mathcal{W}) = 0$. The following theorem takes the first step by providing a necessary condition for globally minimizing the residual loss. We then turn this requirement into a sufficient condition by establishing a set of assumptions. Note that the squared error $l(r)$ is a non-negative convex function of the residuals r , and $l'(r) = 0$ results in $l(r) = 0$. Thus, a critical point $\overline{\mathcal{W}}$ of $\phi_r(\mathbf{x}; \mathcal{W})$ in the parameter space globally minimizes the residual loss if $l'(\mathcal{D}[\hat{u}_{\overline{\mathcal{W}}]}(x) - f(x)) = 0$ for every training sample in \mathbf{x} .

Theorem 1. *For \hat{u} and $\mathcal{D}[\hat{u}]$ as in Lemma 1, a critical point $\overline{\mathcal{W}}$ of the residual loss $\phi_r(\mathbf{x}; \mathcal{W})$ is a global minimum if the following conditions are satisfied:*

1. *Weights \overline{W}_1 of the first layer are strictly non-zero,*
2. *$F_1^{(k)}$ has full row rank, i.e., $\text{rank}(F_1^{(k)}(\mathbf{x})) = N$.*

Theorem 1 distinguishes the global minima from other critical points of the residual loss. However, there is no guarantee that an arbitrary neural network can satisfy the conditions in this theorem. In other words, a critical point that makes $F_1^{(k)}(\mathbf{x})$ full row rank may not exist in the parameter space of a neural network at all. Still, this theorem does give out a necessary condition for such a neural network. Since $F_1^{(k)}(\mathbf{x})$ is an $N \times n_1$ matrix, the width n_1 of the first layer must be at least N for it to be full row rank. In fact, given other assumptions, the next theorem shows that $n_1 \geq N$ is also a sufficient condition for the existence of a global minimum. Note that the first condition on W_1 is satisfied with a high probability in a continuous high-dimensional parameter space.

We first define the non-degenerate critical points used in the next theorem and establish a set of assumptions that connect the two theorems together.

Definition 1 (Non-degenerate Critical Point [Nguyen and Hein, 2017]). *For a function $f \in C^2 : U \subset \mathbb{R}^n \rightarrow \mathbb{R}$ (i.e., f has continuous second-order derivatives), a critical point $x = (x_1, \dots, x_n) \in U$ of f is non-degenerate if its Hessian matrix at x is non-singular. Furthermore, x is non-degenerate on a subset of variables $s \subset \{x_1, \dots, x_n\}$ if the Hessian w.r.t. only the variables in s is non-singular at x .*

Assumptions 1. *For the collocation training data \mathbf{x} of N points, the activation function σ in \hat{u} , and the k -th order differential operator defined in Lemma 1, we assume that*

1. *samples in \mathbf{x} are distinct,*
2. *$\sigma^{(k)}$ is a continuous and strictly monotonically increasing function, and*
3. *$\sigma^{(k)}$ is a bounded function with an infimum of zero.*

Theorem 2. *With Assumptions 1 holding and for $\mathcal{D}[\hat{u}]$ as in Lemma 1, if $n_1 \geq N$, then every critical point $\bar{\mathcal{W}}$ of $\phi_r(\mathbf{x}; \mathcal{W})$ that is non-degenerate on $\{W_2, b_2\}$ is a global minimum of ϕ_r .*

The following remark allows us to make our final conclusion from Theorem 2.

Remark 2. As explained in [Milnor *et al.*, 1965] and [Nguyen and Hein, 2017], for a function f in C^2 that maps an open subset $U \subset \mathbb{R}^n$ to \mathbb{R} , the degenerate critical points in U are rare as the set of all degenerate points has Lebesgue measure zero.

Theorem 2 provides sufficient conditions for a global minimum of the residual loss with a wide network of width N or higher. Based on this theorem, if a PINN with a width of at least N has a non-degenerate critical point, then it also has a global minimum for the residual loss. Since the residual loss $\phi_r(\mathbf{x}; \cdot)$ is a function from $\mathbb{R}^{|\mathcal{W}|}$ to \mathbb{R} and has continuous second derivatives, the degenerate critical points are rare, and the wide PINN in Theorem 2 has a global minimum.

Note that the residual loss is a strong regularizer that results in a data-efficient training process. Thus, PINNs are often trained with $\mathcal{O}(1000)$ collocation points and even fewer boundary data [Raissi *et al.*, 2017; Krishnapriyan *et al.*, 2021]. Therefore, the constraint on the width is well within the practical settings of neural networks. Furthermore, as we observe in the experiments in Section 5, while satisfying the constraint on the width improves the performance, one can expect relatively good results with smaller width as long as the other conditions in Assumptions 1 are almost satisfied.

4 On the Choice of Activation Function

The conditions outlined in Theorem 2 and Assumptions 1 collectively establish an important set of necessities for achieving global minimization of the residual loss. Notably, the requirement of strictly monotonically increasing $\sigma^{(k)}$ implies that it should be a bijection, providing an important guideline in choosing effective activation functions for PINNs. It is noteworthy that bijective activation functions are widely

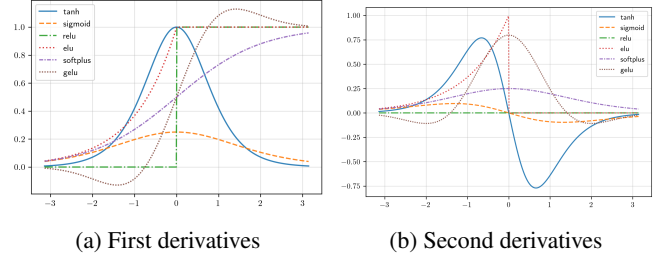


Figure 1: Derivatives of most of the common activation functions are not bijective. Here, only Softplus has a bijective first derivative.

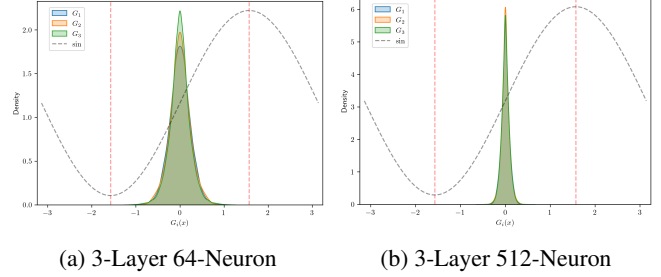


Figure 2: Distribution of the linear outputs of the layers in Sine networks at initialization.

prevalent in deep learning, and extending this characteristic to their derivatives for improved expressiveness in representing differential operators is a plausible goal.

However, the activation functions frequently used in deep learning do not satisfy the bijection property even for the first-order derivatives. As depicted in Figure 1, only Softplus has a bijective first-order derivative, and as we show in Section 5, it indeed improves the performance of the first-order Transport PINN significantly. Meanwhile, there has been an increasing interest in the use of sinusoidal functions either as feature embeddings [Wong *et al.*, 2022; Wang *et al.*, 2021] or activation functions [Sitzmann *et al.*, 2020; Belbute-Peres and Kolter, 2022] for PINNs.

As shown in Figure 2, we observe that the linear outputs of the layers in a neural network with the Sine activation function at initialization are centred at zero with low variance when initialized with normal Xavier initialization. Sitzmann *et al.* [2020] also proposed a uniform initialization scheme for Sine networks that produces normal linear outputs at all layers with a desired variance. Consequently, in both cases, most of the linear outputs of the layers lie in the $[-\pi/2, \pi/2]$ interval where Sine is bijective. Furthermore, as we train the PINNs with the Sine activation function, we observe that layers still exhibit the same behaviour, i.e., most of the linear outputs of the layers are between $-\pi/2$ and $\pi/2$ after convergence, especially as the width grows larger. Figure 3 illustrates the output distributions for each layer of the trained Wave and Klein-Gordon PINNs (We later define these equations in Section 5).

The observations above suggest that the sinusoidal functions can be utilized to almost satisfy the bijective condition of the activation function. Specifically, we use Cosine

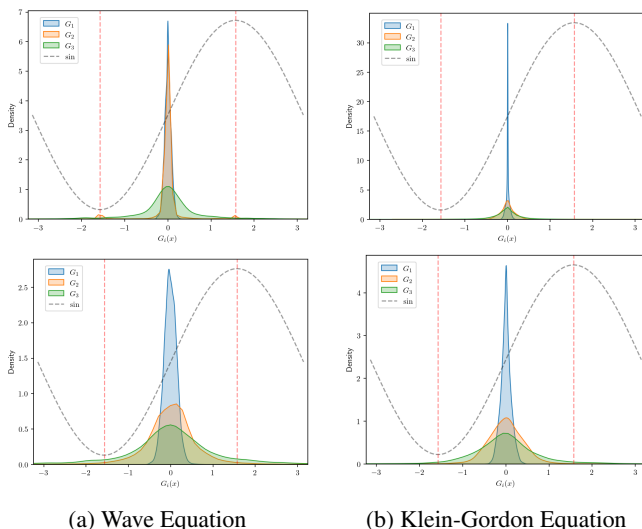


Figure 3: Distribution of linear outputs of PINNs' layers. Top row: 1024 neurons wide, Bottom row: 256 neurons wide

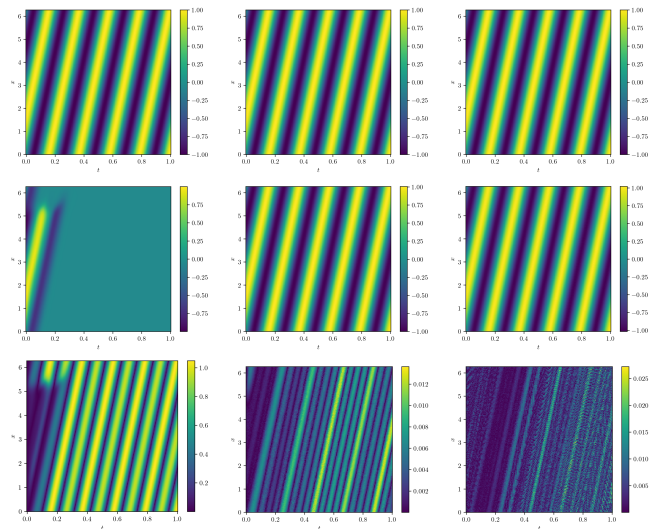
and Sine activation functions to train PINNs with first- and second-order terms, respectively. As a result, as long as the width is adequately large to produce low-variance pre-activations within $[-\pi/2, \pi/2]$, the first-order terms in Cosine networks and the second-order terms in Sine networks are determined with the bijective interval of Sine. The same approach can be taken when solving PDEs with higher odd or even terms.

The experiments in the next section show that sinusoidal non-linearity greatly improves the performance of PINNs compared to the common Tanh activation, and the gains are often greater as the width grows. We note that while the Assumption 1.3 facilitates the proof of the Theorem 2, the crucial property is the bijective $\sigma^{(k)}$, and we relax the assumption on the infimum of the derivatives.

5 Experiments

In this section, we provide numerical results for several PDEs, revealing the impact of the activation functions and the width. We first experiment with the first-order Transport equation, comparing the Softplus and Cosine activation functions with Tanh. Next, we study three second-order PDEs using Sine and Tanh activation functions. We empirically show that Sine significantly improves the performance of PDEs with second-order terms with a noticeable decrease in error as the width exceeds the number of training samples.

In all of the experiments, we use a three-layer feed-forward network with a width varying from 64 neurons up to 1024 neurons and initialized with Normal Xavier initialization. All the models are trained with normalized inputs for 80K epochs using the Adam optimizer and an exponential learning rate decay scheme. The only exception is the Wave equation, for which the models are trained for 120K epochs for better convergence. We repeat each experiment three times with a different random initialization and report the average and the best results.



(a) Tanh 256-Neuron (b) Cosine 256-Neuron (c) Softplus 256-Neuron

Figure 4: Transport Equation. Top panels: Exact solution, Middle panels: Predicted solution, Bottom panels: Absolute Error

5.1 Transport Equation

The transport equation is a first-order linear PDE that describes a quantity as it moves through time and space. We experiment with the one-dimensional equation with the following formulation:

$$\frac{\partial u}{\partial t} + 30 \frac{\partial u}{\partial x} = 0 \quad x \in [0, 2\pi], t \in [0, 1]$$

We also impose a periodic boundary condition $u(t, 0) = u(t, 2\pi)$ and a Dirichlet initial condition $u(0, x)$ consistent with the solution in [Krishnapriyan *et al.*, 2021]. The PINN is then trained with 256 collocation training points and 200 boundary samples. To verify our results in Section 3.3, we choose Softplus as the activation function as it is a smooth version of ReLU with a bijective first derivative equal to the Sigmoid function. We also use Cosine, as it results in a Sine network for the first-order terms.

Table 1 reports the mean absolute errors for the transport equation. In all cases, Softplus and Cosine perform significantly better than Tanh, as shown in Figure 4. Furthermore, as the width becomes equal to the number of collocation samples (256), we observe a noticeable decrease in the absolute error. The same improvement is also evident in the training curve of the residual loss as shown in Figure 5, where the wide models follow a steep curve. For the PINNs with a width of 256 or wider with both Cosine and Softplus activation functions, the absolute errors are between 10^{-2} and 10^{-3} , outperforming the reported 1.1×10^{-2} absolute error achieved with curriculum learning in [Krishnapriyan *et al.*, 2021].

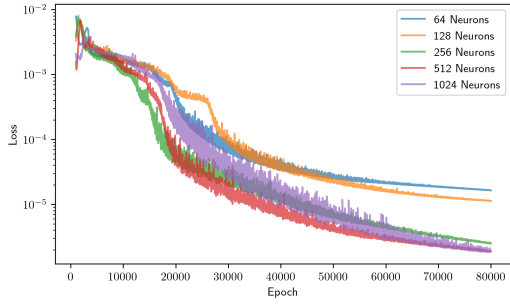


Figure 5: Average residual loss curve for the Transport PINNs with the Softplus activation function and trained with 256 collocation samples.

Width	Tanh		Softplus		Cosine	
	Avg	Best	Avg	Best	Avg	Best
64	0.6314	0.6212	0.0207	0.0111	0.0095	0.0086
128	0.6118	0.6083	0.0229	0.0156	0.0042	0.0039
<u>256</u>	0.5673	0.5588	0.0092	0.0040	0.0029	0.0013
512	0.5168	0.4158	0.0093	0.0062	0.0019	0.0004
1024	0.3632	0.0011	0.0103	0.0062	0.0014	0.0011

Table 1: Average and best mean absolute error for the Transport equation over three random initializations trained with 256 collocation points.

5.2 Wave Equation

The wave equation describes mechanical and electromagnetic waves and has the following form in 1-D:

$$\frac{\partial^2 u}{\partial t^2} = c^2 \frac{\partial^2 u}{\partial x^2}$$

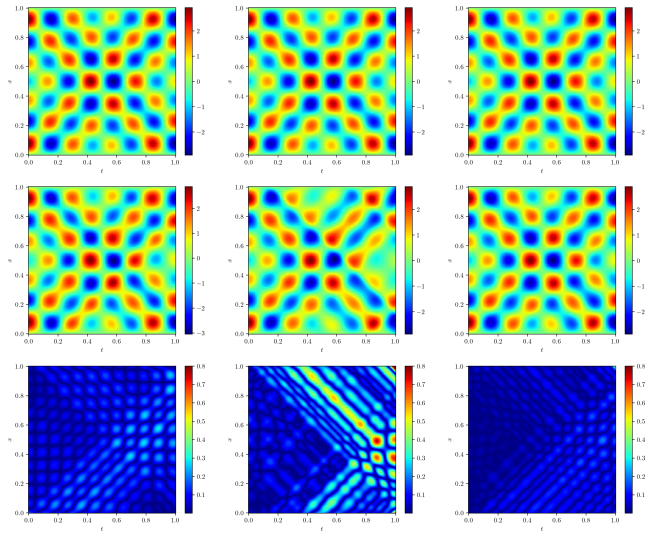
Here c is the velocity of the wave. For $c = 1$ and the solution

$$u(t, x) = \sin(5\pi x) \cos(5\pi t) + 2 \sin(7\pi x) \cos(7\pi t),$$

we train the PINN with 512 collocation points for $t, x \in [0, 1]$ and impose the initial and boundary conditions below with 256 boundary data points:

$$\begin{aligned} u(0, x) &= \sin(5\pi x) + 2 \sin(7\pi x) & x \in [0, 1] \\ \frac{\partial u}{\partial t}(0, x) &= 0 & x \in [0, 1] \\ u(t, 1) &= u(t, 0) = 0 & t \in [0, 1] \end{aligned}$$

The residual loss training curves in Figure 7 highlight the impact of the width in training PINNs, with wider models consistently achieving smaller loss values, and the 512- and 1024-neuron models following almost the same path. This behaviour is similar to the curves in Figure 5 for the transport equation, where all the models with a width of at least N achieve very close loss values. As evident in Table 2, PINNs with both Tanh and Sine activation functions perform notably better than narrow PINNs, with a mean absolute error of 3.11×10^{-2} and 5.62×10^{-2} for Tanh and Sine respectively. Figure 6 illustrates the inability of the narrow Tanh network compared to Sine and wide Tanh models in representing the solution. Also, while narrow Sine PINNs are able to find good solutions, the training is more unstable and the performance is worse on average compared to wider models.



(a) Sine 128-Neuron (b) Tanh 128-Neuron (c) Tanh 1024-Neuron

Figure 6: Wave Equation. Top panels: Exact solution, Middle panels: Predicted solution, Bottom panels: Absolute Error

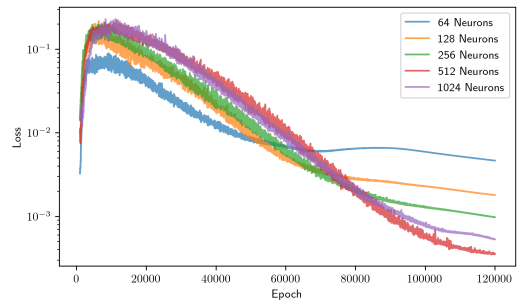


Figure 7: Average residual loss curve for Wave PINNs with the Tanh activation function, trained with 512 collocation samples.

5.3 Helmholtz Equation

We consider a 2D Helmholtz equation of the following form with $t, x \in [-1, 1]$ as in [Wong *et al.*, 2022]:

$$\frac{\partial^2 u}{\partial x^2} + \frac{\partial^2 u}{\partial y^2} + u = (1 - \pi^2 - (6\pi)^2) \sin(\pi x) \cos(6\pi y)$$

With zero boundary conditions, the solution is given by

$$u(x, y) = \sin(\pi x) \sin(6\pi y).$$

The PINN is then trained with 512 collocation points and 256 boundary data, using Sine and Tanh as the activation function. As reported in Table 2, Sine performs remarkably better than Tanh across all widths. Similar to the Wave and Transport equations, there is also a slight decrease in the errors as the width exceeds the number of collocation points. As in the Wave equation, PINNs with the Tanh activation function start to perform better as the width grows larger. However, as illustrated in Figure 8, even the 1024 neurons-wide Tanh network is still unable to capture the solution, while the Sine

Width	Helmholtz				Klein Gordon				Wave			
	Tanh		Sine		Tanh		Sine		Tanh		Sine	
	Avg	Best	Avg	Best	Avg	Best	Avg	Best	Avg	Best	Avg	Best
64	4.7235	4.1456	0.0125	0.0087	0.0275	0.0167	0.0097	0.0059	0.3166	0.2676	0.1966	0.1272
128	2.8161	2.2007	0.0105	0.0064	0.0134	0.0096	0.0056	0.0035	0.2902	0.2351	0.1377	0.0594
256	1.8516	1.4016	0.0273	0.0212	<u>0.0606</u>	<u>0.0191</u>	0.0052	<u>0.0031</u>	0.1937	0.1808	0.3608	0.0676
512	<u>0.7854</u>	<u>0.4909</u>	0.0044	<u>0.0028</u>	0.0875	0.0289	0.0096	0.0049	<u>0.1577</u>	<u>0.0725</u>	0.0604	<u>0.0587</u>
1024	0.5946	0.2221	0.0067	0.0056	0.1939	0.0928	0.0090	0.0046	0.1147	0.0311	0.0620	0.0562

Table 2: Average and best mean absolute errors for second-order PDEs over three random initializations. Underlined values show where the width is equal to N .

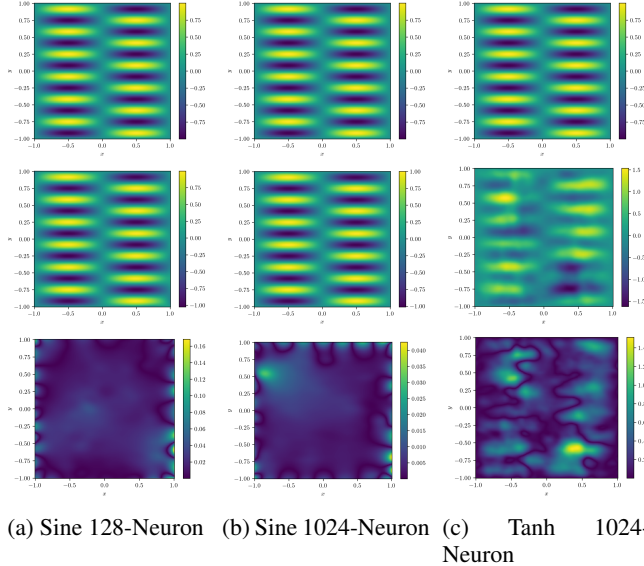


Figure 8: Helmholtz Equation. Top panels: Exact solution, Middle panels: Predicted solution, Bottom panels: Absolute Error

network finds an acceptable solution even with a width of 128 neurons.

5.4 Klein-Gordon Equation

We conduct the same experiments on the non-linear one-dimensional Klein-Gordon equation of the following form:

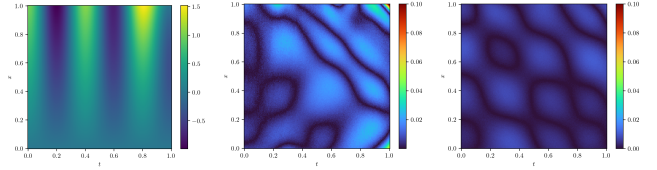
$$\frac{\partial^2 u}{\partial t^2} - \frac{\partial^2 u}{\partial x^2} + u^3 = f(t, x), \quad x \in [0, 1], t \in [0, 1]. \quad (6)$$

We adopt the solution provided in [Wang *et al.*, 2020a] and derive the source term $f(t, x)$ in Eq. 6 to be consistent with the solution below:

$$u(t, x) = x \cos(5\pi t) + (xt)^3$$

The model is then trained with a zero initial condition and a Dirichlet boundary condition corresponding to the solution u , using 256 collocation training points and 200 boundary data.

The resulting absolute errors are reported in Table 2. Similar to other equations, the Sine activation function performs consistently better for all widths, achieving the best mean absolute error of 3.1×10^{-3} with the 256 neurons-wide model.



(a) Exact Solution (b) Tanh 128-Neuron (c) Sine 256-Neuron

Figure 9: Absolute error of the Klein-Gordon PINNs.

Tanh also performs reasonably well with the 128 neurons-wide model, although it still performs slightly worse than the Sine models, as shown in Figure 9.

6 Conclusion

The differentiation process in the residual loss of PINNs transforms the structure of the neural networks and their outputs, rendering the existing theory around loss functions and common supervised tasks ineffective in analyzing PINNs. In this work, we aim to fill the gap in our understanding of the residual loss and derive the requirements in network design that lead to achieving global minimization of this loss function. To this end, we study the residual loss at a critical point in the parameter space of the neural network and look for distinct characteristics of a global minimum that sets it apart from other critical points. We then use those characteristics to derive the requirements in the neural network design that ensure the existence of a global minimum. In particular, we show that under certain conditions, wide networks globally minimize the residual loss. Additionally, we reveal that activation functions with well-behaved high-order derivatives are crucial in the optimal minimization of the residual loss. We then use the established theory and empirical observations to choose activation functions and verify their effectiveness by conducting a set of experiments. The theory developed in this work paves the way for further development of better activation functions and provides a guideline for designing effective PINNs.

Acknowledgements

This research is supported by Natural Sciences and Engineering Research Council of Canada (NSERC), Discovery Grants program, and the Vector Scholarship in Artificial Intelligence, provided through the Vector Institute.

References

- [Allen-Zhu *et al.*, 2019] Zeyuan Allen-Zhu, Yuanzhi Li, and Zhao Song. A convergence theory for deep learning via over-parameterization. In *International conference on machine learning*, pages 242–252. PMLR, 2019.
- [Belbute-Peres and Kolter, 2022] Filipe de Avila Belbute-Peres and J Zico Kolter. Simple initialization and parametrization of sinusoidal networks via their kernel bandwidth. *arXiv preprint arXiv:2211.14503*, 2022.
- [Cai *et al.*, 2021] Shengze Cai, Zhiping Mao, Zhicheng Wang, Minglang Yin, and George Em Karniadakis. Physics-informed neural networks (pinns) for fluid mechanics: A review. *Acta Mechanica Sinica*, 37(12):1727–1738, 2021.
- [Chen *et al.*, 2020a] Yuyao Chen, Lu Lu, George Em Karniadakis, and Luca Dal Negro. Physics-informed neural networks for inverse problems in nano-optics and meta-materials. *Optics express*, 28(8):11618–11633, 2020.
- [Chen *et al.*, 2020b] Zixiang Chen, Yuan Cao, Quanquan Gu, and Tong Zhang. A generalized neural tangent kernel analysis for two-layer neural networks. *Advances in Neural Information Processing Systems*, 33:13363–13373, 2020.
- [Dong and Ni, 2021] Suchuan Dong and Naxian Ni. A method for representing periodic functions and enforcing exactly periodic boundary conditions with deep neural networks. *Journal of Computational Physics*, 435:110242, 2021.
- [Du and Hu, 2019] Simon Du and Wei Hu. Width provably matters in optimization for deep linear neural networks. In *International Conference on Machine Learning*, pages 1655–1664. PMLR, 2019.
- [Du *et al.*, 2019] Simon Du, Jason Lee, Haochuan Li, Liwei Wang, and Xiyu Zhai. Gradient descent finds global minima of deep neural networks. In *International conference on machine learning*, pages 1675–1685. PMLR, 2019.
- [Farhani *et al.*, 2022] G. Farhani, Alexander Kazachek, and Boyu Wang. Momentum diminishes the effect of spectral bias in physics-informed neural networks. *arXiv preprint arXiv:2206.14862*, 2022.
- [Jacot *et al.*, 2018] Arthur Jacot, Franck Gabriel, and Clément Hongler. Neural tangent kernel: Convergence and generalization in neural networks. *Advances in neural information processing systems*, 31, 2018.
- [Krishnapriyan *et al.*, 2021] Aditi Krishnapriyan, Amir Gholami, Shandian Zhe, Robert Kirby, and Michael W Mahoney. Characterizing possible failure modes in physics-informed neural networks. *Advances in Neural Information Processing Systems*, 34:26548–26560, 2021.
- [Lee *et al.*, 2019] Jaehoon Lee, Lechao Xiao, Samuel Schoenholz, Yasaman Bahri, Roman Novak, Jascha Sohl-Dickstein, and Jeffrey Pennington. Wide neural networks of any depth evolve as linear models under gradient descent. *Advances in neural information processing systems*, 32, 2019.
- [Li *et al.*, 2020] Zongyi Li, Nikola Kovachki, Kamyar Azizzadenesheli, Burigede Liu, Kaushik Bhattacharya, Andrew Stuart, and Anima Anandkumar. Fourier neural operator for parametric partial differential equations. *arXiv preprint arXiv:2010.08895*, 2020.
- [Liu *et al.*, 2020] Chaoyue Liu, Libin Zhu, and Misha Belkin. On the linearity of large non-linear models: when and why the tangent kernel is constant. *Advances in Neural Information Processing Systems*, 33:15954–15964, 2020.
- [McClenny and Braga-Neto, 2020] Levi McClenny and Ulisses Braga-Neto. Self-adaptive physics-informed neural networks using a soft attention mechanism. *arXiv preprint arXiv:2009.04544*, 2020.
- [Meronen *et al.*, 2021] Lassi Meronen, Martin Trapp, and Arno Solin. Periodic activation functions induce stationarity. *Advances in Neural Information Processing Systems*, 34:1673–1685, 2021.
- [Milnor *et al.*, 1965] John Milnor, L. Siebenmann, and J. Sondow. *Lectures on the H-Cobordism Theorem*. Princeton University Press, 1965.
- [Nguyen and Hein, 2017] Quynh Nguyen and Matthias Hein. The loss surface of deep and wide neural networks. In *International conference on machine learning*, pages 2603–2612. PMLR, 2017.
- [Nguyen and Mondelli, 2020] Quynh N Nguyen and Marco Mondelli. Global convergence of deep networks with one wide layer followed by pyramidal topology. *Advances in Neural Information Processing Systems*, 33:11961–11972, 2020.
- [Oymak and Soltanolkotabi, 2020] Samet Oymak and Mahdi Soltanolkotabi. Toward moderate overparameterization: Global convergence guarantees for training shallow neural networks. *IEEE Journal on Selected Areas in Information Theory*, 1(1):84–105, 2020.
- [Rahaman *et al.*, 2018] Nasim Rahaman, A. Baratin, Devansh Arpit, Felix Dräxler, Min Lin, F. Hamprecht, Yoshua Bengio, and Aaron C. Courville. On the spectral bias of neural networks. *International Conference On Machine Learning*, 2018.
- [Raissi *et al.*, 2017] Maziar Raissi, Paris Perdikaris, and George Em Karniadakis. Physics informed deep learning (part i): Data-driven solutions of nonlinear partial differential equations. *arXiv preprint arXiv:1711.10561*, 2017.
- [Reiser *et al.*, 2022] Patrick Reiser, Marlen Neubert, André Eberhard, Luca Torresi, Chen Zhou, Chen Shao, Houssam Metni, Clint van Hoesel, Henrik Schopmans, Timo Sommer, et al. Graph neural networks for materials science and chemistry. *Communications Materials*, 3(1):93, 2022.
- [Safran and Shamir, 2016] Itay Safran and Ohad Shamir. On the quality of the initial basin in overspecified neural networks. In *International Conference on Machine Learning*, pages 774–782. PMLR, 2016.
- [Sirignano and Spiliopoulos, 2018] Justin Sirignano and Konstantinos Spiliopoulos. Dgm: A deep learning algo-

- rithm for solving partial differential equations. *Journal of computational physics*, 375:1339–1364, 2018.
- [Sitzmann *et al.*, 2020] Vincent Sitzmann, Julien Martel, Alexander Bergman, David Lindell, and Gordon Wetzstein. Implicit neural representations with periodic activation functions. *Advances in neural information processing systems*, 33:7462–7473, 2020.
- [Wang *et al.*, 2020a] Sifan Wang, Yujun Teng, and Paris Perdikaris. Understanding and mitigating gradient pathologies in physics-informed neural networks. *arXiv preprint arXiv:2001.04536*, 2020.
- [Wang *et al.*, 2020b] Sifan Wang, Xinling Yu, and P. Perdikaris. When and why pinns fail to train: A neural tangent kernel perspective. *Journal Of Computational Physics*, 2020.
- [Wang *et al.*, 2021] Sifan Wang, Hanwen Wang, and Paris Perdikaris. On the eigenvector bias of fourier feature networks: From regression to solving multi-scale pdes with physics-informed neural networks. *Computer Methods in Applied Mechanics and Engineering*, 384:113938, 2021.
- [Wang *et al.*, 2022] Sifan Wang, Shyam Sankaran, and Paris Perdikaris. Respecting causality is all you need for training physics-informed neural networks. *arXiv preprint arXiv:2203.07404*, 2022.
- [Wight and Zhao, 2020] Colby L Wight and Jia Zhao. Solving allen-cahn and cahn-hilliard equations using the adaptive physics informed neural networks. *arXiv preprint arXiv:2007.04542*, 2020.
- [Wong *et al.*, 2022] Jian Cheng Wong, Chinchun Ooi, Abhishek Gupta, and Yew-Soon Ong. Learning in sinusoidal spaces with physics-informed neural networks. *IEEE Transactions on Artificial Intelligence*, 2022.
- [Zhang *et al.*, 2022] Jie Zhang, Yihui Zhao, Fergus Shone, Zhenhong Li, Alejandro F Frangi, Sheng Quan Xie, and Zhi-Qiang Zhang. Physics-informed deep learning for musculoskeletal modeling: Predicting muscle forces and joint kinematics from surface emg. *IEEE Transactions on Neural Systems and Rehabilitation Engineering*, 31:484–493, 2022.

A Generalizing to Multiple Independent Variables

We first generalize Lemmas 1 and 2 and Theorem 1 in Section 3 to multiple (d) independent variables and present the proofs for them, and then, prove Theorem 2 in the next section. We consider a function of d independent variables and a differential operator \mathcal{D} with k -th order terms and coefficients c_1, \dots, c_d of the following form:

$$\mathcal{D}[u] = c_1 \frac{\partial^k u}{\partial x_1^k} + \dots + c_d \frac{\partial^k u}{\partial x_d^k} \quad (7)$$

We also define $(W_1)_i \in \mathbb{R}^{1 \times n_1}$ for $i \in \{1, \dots, d\}$ to represent the i -th row of the weight matrix W_1 , i.e., $(W_1)_i$ are the weights corresponding to the i -th input variable.

Lemma 3 (Generalization of Lemma 1). *For a two-layer neural network \hat{u} of d input variables and the k -th order differential operator in Eq. 7, $\mathcal{D}[\hat{u}]$ is given by*

$$\mathcal{D}[\hat{u}](x) = W_2^\top \times (F_1^{(k)}(x) \circ (c_1(W_1)_1^k + \dots + c_d(W_1)_d^k))^\top.$$

Proof. Note that the neural network is defined as

$$\begin{aligned} \hat{u}(x) &= F_1(x) \times W_2 + b_2 \\ &= \sigma(G_1(x)) \times W_2 + b_2, \quad G_1(x) = x \times W_1 + b_1 \end{aligned}$$

The first derivative $\frac{\partial \hat{u}}{\partial x_1}$ w.r.t. the first input variable is then derived as follows:

$$\begin{aligned} \frac{\partial \hat{u}}{\partial x_1} &= \frac{\partial \hat{u}}{\partial F_1} \times \left(\frac{\partial F_1}{\partial G_1} \frac{\partial G_1}{\partial x_1} \right) \\ &= W_2^\top \times \left(\frac{\partial F_1}{\partial G_1} \frac{\partial G_1}{\partial x_1} \right) \end{aligned} \quad (8)$$

Derivative of F_1 w.r.t. G_1 is just $\sigma'(G_1(x))$. We also have

$$\begin{aligned} G_1(x) &= x \times W_1 + b_1 \\ &= \sum_{i=1}^d x_i (W_1)_i + b_1. \end{aligned}$$

Thus, Eq. 8 yields:

$$\frac{\partial \hat{u}}{\partial x_1} = W_2^\top \times (\sigma'(G_1(x)) \circ (W_1)_1)^\top$$

For higher-order derivatives, only $G_1(x)$ depends on x_1 , and other terms are constants. Hence, assuming that the $(k-1)$ -th derivative is given by $W_2^\top \times (\sigma^{(k-1)}(G_1(x)) \circ (W_1)_1^{k-1})^\top$, the k -th derivative is

$$\begin{aligned} \frac{\partial^k \hat{u}}{\partial x_1^k} &= W_2^\top \times \left(\frac{\partial F_1^{(k-1)}}{\partial x_1} \circ (W_1)_1^{k-1} \right)^\top \\ &= W_2^\top \times \left(\sigma^{(k)}(G_1(x)) \circ (W_1)_1 \circ (W_1)_1^{k-1} \right)^\top \\ &= W_2^\top \times \left(F_1^{(k)}(x) \circ (W_1)_1^k \right)^\top. \end{aligned}$$

Derivatives w.r.t. other input variables are taken similarly. Thus, the differential operator $\mathcal{D}[\hat{u}]$ is

$$\begin{aligned} \mathcal{D}[\hat{u}](x) &= \sum_{i=1}^d c_i W_2^\top \times \left(F_1^{(k)}(x) \circ (W_1)_i^k \right)^\top \\ &= W_2^\top \times \left(\sum_{i=1}^d c_i F_1^{(k)}(x) \circ (W_1)_i^k \right)^\top \\ &= W_2^\top \times \left(F_1^{(k)}(x) \circ \sum_{i=1}^d c_i (W_1)_i^k \right)^\top. \end{aligned}$$

□

Note that Lemma 3 (and other results in this section) can be further generalized to include mixed derivatives such as

$$\frac{\partial^2 \hat{u}}{\partial x_1 \partial x_2} = W_2^\top \times (F_1^{(k)}(x) \circ (W_1)_1 \circ (W_1)_2)^\top,$$

which we don't consider for simplicity.

Lemma 4 (Generalization of Lemma 2). *For \hat{u} and $\mathcal{D}[\hat{u}]$ as in Lemma 3, gradients of the residual loss w.r.t. the weights of the second layer over the training collocation data \mathbf{x} of N samples are given by*

$$\begin{aligned} \nabla_{W_2} \phi_r(\mathbf{x}; \mathcal{W}) &= \\ &= \left(\sum_{i=1}^d c_i (W_1)_i^k \right) \circ \left(l'(\mathcal{D}[\hat{u}](\mathbf{x}) - f(\mathbf{x}))^\top \times F_1^{(k)}(\mathbf{x}) \right). \end{aligned}$$

Proof. Let $A \in \mathbb{R}^{1 \times n_1}$ be $\sum_{i=1}^d c_i (W_1)_i^k$. From Lemma 3, the residual loss over collocation samples $\mathbf{x} = [x^1, \dots, x^N]^\top$ is given by

$$\begin{aligned} \phi_r(\mathbf{x}; \mathcal{W}) &= \sum_{i=1}^N l \left(W_2^\top \times (F_1^{(k)}(x^i) \circ A) - f(x^i) \right) \\ &= \sum_{i=1}^N l \left(\sum_{j=1}^{n_1} (W_2)_j (F_{1j}^{(k)}(x^i) A_j) - f(x^i) \right), \end{aligned}$$

where $F_{1j}^{(k)}$ is the scalar output of neuron j in the first layer fed to $\sigma^{(k)}$, and A_j and $(W_2)_j$ are the j -th elements of the row and column vectors A and W_2 (note that $W_2 \in \mathbb{R}^{n_1 \times 1}$). Let $r_i \in \mathbb{R}$ denote the residual $\sum_{j=1}^{n_1} (W_2)_j (F_{1j}^{(k)}(x^i) A_j) - f(x^i)$ for a sample $x^i \in \mathbf{x}$. The partial derivative $\frac{\partial \phi_r}{\partial (W_2)_\alpha}$ for $\alpha \in \{1, \dots, n_1\}$ is then derived as

$$\begin{aligned} \frac{\partial \phi_r}{\partial (W_2)_\alpha}(\mathbf{x}; \mathcal{W}) &= \sum_{i=1}^N \frac{\partial l(r_i)}{\partial r_i} \frac{\partial r_i}{\partial (W_2)_\alpha} \\ &= \sum_{i=1}^N l'(r_i) F_{1\alpha}^{(k)}(x^i) A_\alpha \\ &= A_\alpha \sum_{i=1}^N l'(r_i) F_{1\alpha}^{(k)}(x^i), \end{aligned}$$

and the gradients w.r.t. W_2 are

$$\begin{aligned}\nabla_{W_2} \phi_r(\mathbf{x}; \mathcal{W}) &= \begin{bmatrix} A_1 \sum_{i=1}^N l'(r_i) F_{11}^{(k)}(x^i) \\ \vdots \\ A_{n_1} \sum_{i=1}^N l'(r_i) F_{1n_1}^{(k)}(x^i) \end{bmatrix}^\top \\ &= A \circ \begin{bmatrix} \sum_{i=1}^N l'(r_i) F_{11}^{(k)}(x^i) \\ \vdots \\ \sum_{i=1}^N l'(r_i) F_{1n_1}^{(k)}(x^i) \end{bmatrix}^\top \\ &= A \circ \left(\sum_{i=1}^N l'(r_i) F_1^{(k)}(x^i) \right) \\ &= A \circ (L'^\top \times F_1^{(k)}(\mathbf{x})),\end{aligned}$$

where $L' \in \mathbb{R}^N$ is $[l'(r_1), \dots, l'(r_N)]^\top$. \square

Theorem 3 (Generalization of Theorem 1). *For \hat{u} and $\mathcal{D}[\hat{u}]$ as in Lemma 3, a critical point \overline{W} of the residual loss $\phi_r(\mathbf{x}, \mathcal{W})$ is a global minimum if the following conditions are satisfied:*

1. *The summation $\sum_{i=1}^d c_i (\overline{W}_1)_i^k$ of the weights of each input variable in the first layer is strictly non-zero,*
2. *$F_1^{(k)}$ has full row rank, i.e., $\text{rank}(F_1^{(k)}(\mathbf{x})) = N$.*

Proof. At a critical point \overline{W} of ϕ_r , the gradients of ϕ_r w.r.t. the weights of the second layer are zero. Let $L' \in \mathbb{R}^N$ be $l'(\mathcal{D}[\hat{u}_{\overline{W}}](\mathbf{x}) - f(\mathbf{x}))$ and $A \in \mathbb{R}^{1 \times n_1}$ be $\sum_{i=1}^d c_i (\overline{W}_1)_i^k$. Lemma 4 yields

$$\nabla_{W_2} \phi_r(\mathbf{x}; \overline{W}) = A \circ (L'^\top \times F_1^{(k)}(\mathbf{x})) = 0.$$

Since A is strictly non-zero, $L'^\top \times F_1^{(k)}(\mathbf{x})$ must be zero. Furthermore, if $F_1^{(k)}(\mathbf{x})$ has full row rank, the null space of its transpose is zero, and thus, L' must be zero for the above product to hold. Since l is convex, $l(\mathcal{D}[\hat{u}_{\overline{W}}](\mathbf{x}) - f(\mathbf{x}))$ and $\phi_r(\mathbf{x}; \overline{W})$ are also zero, and \overline{W} globally minimizes the residual loss. \square

B Proof of Theorem 2

In this section, we present a brief explanation of the proof for Theorem 2. We refer the readers to [Nguyen and Hein, 2017, Section 4] for complete and more detailed proof, while we provide the necessary modifications for PINNs here. Note that in [Nguyen and Hein, 2017] it is shown that a global minimum for a normal neural network is achieved when $[F_1(\mathbf{x}), \mathbf{1}_N]$ is full row rank, and then, a width of $n_1 \geq N - 1$ is shown to be sufficient. For PINNs, we showed that $F_1^{(k)}(\mathbf{x})$ should be full row rank for globally minimizing the residual loss and a width of $n_1 \geq N$ is sufficient.

In summary, the proof works by first showing that a parameterization of the neural network that results in full row-rank $F_1^{(k)}(\mathbf{x})$ does exist. Based on the fact that $F_1^{(k)}(\mathbf{x})$ and determinants of its sub-matrices are real-analytic functions of

the model parameters, it is then shown that for any set of parameters $\{W_1, b_1\}$ that $F_1^{(k)}(\mathbf{x})$ is not full row-rank, there exists another set of parameters in a ball of any positive radius around $\{W_1, b_1\}$ that results in $\text{rank}(F_1^{(k)}(\mathbf{x})) = N$. Finally, using the implicit function theorem and the non-degeneracy of the critical point on $\{W_2, b_2\}$, it is shown that there exists another critical point in a ball of an arbitrarily small radius around the original critical point that results in full row rank $F_1^{(k)}(\mathbf{x})$.

We start by modifying Lemma 4.3 in [Nguyen and Hein, 2017], showing that $F_1^{(k)}(\mathbf{x})$ can be full row-rank for some parameters in the parameter space when $n_1 \geq N$.

Lemma 5 (Existence of full row-rank $F_1^{(k)}(\mathbf{x})$). *With Assumptions 1 holding and for a two-layer neural network with a width $n_1 \geq N$, there exists a parameterization that results in $\text{rank}(F_1^{(k)}(\mathbf{x})) = N$*

Proof. Following the proof in [Nguyen and Hein, 2017], we construct the parameters $\{W_1, b_1\}$ such that $F_1^{(k)}$ is full row-rank. Since $n_1 \geq N$ and $F_1^{(k)}(\mathbf{x}) \in \mathbb{R}^{N \times n_1}$, N columns from $F_1^{(k)}$ must be linearly independent for it to have rank N . We denote the sub-matrix containing the first N columns with A and the other $n_1 - N$ columns with B . Showing that the matrix A is full rank for a set of parameters proves the argument as the original matrix $F_1^{(k)}(\mathbf{x}) = [A \ B]$ contains the same N linearly independent columns in A .

Pick a vector $a \in \mathbb{R}^d$ such that

$$a \cdot x^1 < a \cdot x^2 < \dots < a \cdot x^N \quad (a \cdot x^i \text{ denotes dot product}) \quad (9)$$

Note that by Assumption 1.1, the rows of the inputs $\mathbf{x} = [x^1, \dots, x^N]^\top$ are distinct. Thus, for some $i, j \in \{1, \dots, N\}$ that $i \neq j$, the set $\{a \in \mathbb{R}^d \mid a \cdot (x^i - x^j) = 0\}$ is a hyperplane with Lebesgue measure zero. For all pairs of distinct samples in \mathbf{x} , there are $N(N-1)/2$ such hyperplanes, and their union still has Lebesgue measure zero. As a result, a vector a that results in the inequality above does exist.

By Assumption 1.3, the infimum of $\sigma^{(k)}$ is zero. Also, let γ denote the supremum of $\sigma^{(k)}$. Thus, $\lim_{x \rightarrow -\infty} \sigma^{(k)}(x) = 0$ and $\lim_{x \rightarrow \infty} \sigma^{(k)}(x) = \gamma$ as $\sigma^{(k)}$ is strictly monotonically increasing. Pick any $\beta \in \mathbb{R}$. Since $\sigma^{(k)}$ is strictly monotonically increasing, $\sigma^{(k)}(\beta)$ is greater than the infimum zero. For $\alpha \in \mathbb{R}$, the weights and biases of the first N neurons in the first layer are defined as $w_j = -\alpha a$ and $b_j = \alpha x^j \cdot a + \beta$ for $j \in \{1, \dots, N\}$, as in [Nguyen and Hein, 2017]. With this choice of weights, the outputs A of the first N neurons become a function of α with $A(\alpha)_{ij} = \sigma^{(k)}(x^i \cdot w_j + b_j) = \sigma^{(k)}(\alpha(x^j - x^i) \cdot a + \beta)$ being the output of the j -th neuron for the i -th sample for $i, j \in \{1, \dots, N\}$. Based on the ordering in Eq. 9, $A(\alpha)$ at the limit becomes:

$$\lim_{\alpha \rightarrow \infty} A(\alpha) = \begin{bmatrix} \sigma^{(k)}(\beta) & \gamma & \gamma & \dots & \gamma \\ 0 & \sigma^{(k)}(\beta) & \gamma & \dots & \gamma \\ 0 & 0 & \sigma^{(k)}(\beta) & \dots & \gamma \\ \vdots & \vdots & \vdots & \ddots & \vdots \\ 0 & 0 & 0 & \dots & \sigma^{(k)}(\beta) \end{bmatrix}$$

The matrix above is upper triangular with a positive diagonal, and thus, it has a positive determinant and is full rank.

The rest of the proof is identical to [Nguyen and Hein, 2017]. As the determinant of $A(\alpha)$ is a polynomial function of its entries and is continuous in α , for some $\alpha_0 \in \mathbb{R}$, $A(\alpha)$ has a positive determinant and is full rank for all $\alpha > \alpha_0$. Thus, the weights of the first N neurons in the first layer can be chosen in a way that results in a full row rank $F_1^{(k)}(\mathbf{x})$, regardless of the weights of other neurons. \square

The rest of the proof for Theorem 2 can be adapted from [Nguyen and Hein, 2017, Section 4] by replacing $[F_1(\mathbf{x}), \mathbf{1}_N]$ with $F_1^{(k)}(\mathbf{x})$ and subtle modifications. Thus, we briefly go through the proof without formally presenting the details. The proof continues by observing that $F_1^{(k)}(\mathbf{x})$ is a real analytic function of parameters $\{W_1, b_1\}$ (as long as $\sigma^{(k)}$ is real analytic), as it is a composition of linear transformations, multiplications, and addition, which are all real analytic, with the real analytic $\sigma^{(k)}$. Similarly, the determinants of the $N \times N$ sub-matrices of $F_1^{(k)}(\mathbf{x})$ are also polynomial functions of the parameters and are real analytic. As proven in [Nguyen and Hein, 2017, Lemma 4.4], the last argument on determinants and Lemma 5 conclude that the set $\{\{W_1, b_1\} \mid \text{rank}(F_1^{(k)}(\mathbf{x})) < N\}$ has Lebesgue measure zero. This is because, for a real analytic function that is not constantly zero, the set of parameters that make it zero has Lebesgue measure zero. Since the determinant function is real analytic and is not constant zero, as shown in Lemma 5, the set of parameters that make it zero has Lebesgue measure zero. Consequently, for any set of parameters $\{W'_1, b'_1\}$ that $\text{rank}(F_1^{(k)}(\mathbf{x})) < N$, the ball centred at $\{W'_1, b'_1\}$ with any radius $\epsilon > 0$ contains at least one $\{W_1, b_1\}$ such that $\text{rank}(F_1^{(k)}(\mathbf{x})) = N$ [Nguyen and Hein, 2017, Corollary 4.5].

Using the implicit function theorem, it is then shown that for a critical point $\bar{W} = \{\bar{W}_1, \bar{b}_1, \bar{W}_2, \bar{b}_2\}$ that is non-degenerate on $\{W_2, b_2\}$, there exists an open ball around $\{\bar{W}_1, \bar{b}_1\}$ for some radius $\delta_1 > 0$ that for every $\{W'_1, b'_1\}$ in the ball, $\{W'_1, b'_1, \bar{W}_2, \bar{b}_2\}$ is also a critical point. Moreover, as we discussed before, for every $0 < \delta_2 \leq \delta_1$, there is a ball of radius δ_2 around $\{W'_1, b'_1\}$ that contains at least one set of parameters $\{\tilde{W}_1, \tilde{b}_1\}$ that satisfies $\text{rank}(F_1^{(k)}(\mathbf{x})) = N$. Note that $\{\tilde{W}_1, \tilde{b}_1, \bar{W}_2, \bar{b}_2\}$ is still a critical point as well. Nguyen et al. [2017] further show how $\{\tilde{W}_1, \tilde{b}_1\}$ are equal to the original $\{\bar{W}_1, \bar{b}_1\}$ as the radius of the ball approaches zero.

With the results above, we get a critical point that makes $F_1^{(k)}$ full-rank. Based on Theorems 1 and 3, the resulting critical point is also a global minimum as long as the condition on the sum of weights is also satisfied. Note that the rarity of degenerate critical points (as explained in Section 3.3) means that non-degenerate ones are the common type of critical points when $n_1 \geq N$. Thus, the conditions on the sum of the weights of the first layer are also satisfied for most of the non-degenerate critical points with a high probability.

	TT	TS	W	K	H
128	0.613	0.011	0.406	0.024	0.590
256	0.625	0.050	0.135	0.071	0.762
512	0.627	0.002	0.046	0.089	0.502
1024	0.654	0.668	0.024	0.118	0.443

Table 3: MAE from sf-PINN. TT: Transport with Tanh, TS: Transport with Softplus, W: Wave, K: Klein-Gordon, H: Helmholtz

	Navier-Stokes			Burger’s		
W	T	SF-T	S	T	SF-T	S
64	0.047	0.009	0.010	0.010	0.099	0.014
128	0.010	0.010	0.011	0.013	0.046	0.034
256	0.007	0.013	0.010	0.053	0.060	0.027

Table 4: MAEs for Lid-driven Cavity ($Re = 400$) and Burger’s equation with vanilla Tanh MLP (T), sf-PINN with Tanh (SF-T), and Sine MLP (S).

C Comparison with Sinusoidal Features

Applying random or trainable sinusoidal embeddings on PINN inputs has been explored before [Wong *et al.*, 2022; Wang *et al.*, 2020b]. In particular, the first layer in sf-PINN uses $\sin(2\pi x)$ as the activation function, followed by other layers with any activation function of choice [Wong *et al.*, 2022]. To confirm the effectiveness of the Sine activation function compared to Sine features in sf-PINN, we trained sf-PINNs for the equations in Section 5.

Table 3 reports the MAEs from sf-PINN for each equation. Compared to Tables 1 and 2, we observe that in most cases, our results outperform sf-PINN. Note that, consistent with Section 3, Softplus activation significantly improves the performance of sf-PINNs for the Transport equation, underpinning our findings about the activation functions. In the case of the Wave equation, sf-PINN with Tanh performs better than plain Sine MLP, though the condition on width still improves the performance as the number of neurons grows beyond the number of collocation points ($N = 512$).

D Non-linear PDEs

Our theoretical analysis primarily focused on linear PDEs, and we empirically showed the effectiveness of our findings for solving linear PDEs. We also tried the non-linear Klein-Gordon equation in Section 5.4 and demonstrated the effectiveness of our method for solving this equation. However, as apparent in Table 2, the gains for the Klein-Gordon equation are not as significant and consistent as other linear equations, especially regarding the width.

To better understand to what extent our findings generalize to non-linear equations, we perform similar experiments with the non-linear Burger’s equation and steady-state Navier-Stokes (lid-driven cavity flow with $Re = 400$). Table 4 reports the MAEs for each equation. Similar to our observations from the Klein-Gordon equation, the gains from the width and Sine activation are not as consistent as linear equations. For the Navier-Stokes equation, while the Sine MLP

performs consistently well across all various widths, the Tanh MLP eventually outperforms both sf-PINN and Sine MLP as the width grows. With Burger's equation, the Tanh MLP performs best with a narrow network and degrades as the width grows, while the Sine MLP fluctuates closely.

Altogether, our experiments suggest that while the conditions discussed for linear equations can partly improve the performance of non-linear PINNs, non-linear equations come with intricacies regarding the representation power and optimization of PINNs that require further analysis.